Numerical simulations of cardiac arrhythmias and defibrillation

M. Hanslien, J. Sundnes and G.T. Lines

Simula Research Laboratory and Department of Informatics, University of Oslo

Abstract

This paper is concerned with simulation of cardiac arrhythmias and defibrillation. A model is outlined which combines the bidomain model for the electrical activity with a non-linear elasticity equation for the mechanical properties of the tissue. The result is a highly complex mathematical model, for which it is hard to construct efficient solution techniques. The difficulty of performing accurate numerical simulations is further increased by the fast dynamics of the electrophysiology equations, which lead to strict resolution requirements in space and time. Applying the defibrillation shock to the heart tissue further increases these problems. We present an efficient numerical algorithm for the electrophysiology model, which is a coupled system of non-linear PDEs and ODEs. An operator splitting method is combined with implicit time discretization and a standard Galerkin finite element solver, leading to a block structured linear system to be solved for each time step. The system is solved with a conjugate gradient and a block preconditioner based on multigrid.

INTRODUCTION

Ventricular fibrillation is the main cause of sudden cardiac death, which is the most frequent cause of death in the developed world. Fibrillation, a severe form of cardiac arrhythmia, is seen as a disorganized pattern of electrical activation in the heart, taking the form of a spiral wave, tiny wavelets, or a mix of the two, see e.g. Chen et al (2003). The disturbance of the normal rhythmic electrical activity causes inadequate contraction, and in the ultimate stage the contraction is completely stalled. Ventricular fibrillation is lethal if not treated within a few minutes.

The most common cause of ventricular fibrillation is a heart attack (infarction). This condition, caused by insufficient blood supply to parts of the heart muscle, leads to abnormal heterogeneities in the heart muscle. Both electrophysiological and mechanical properties of the tissue are affected by the reduced supply of blood. In particular, the muscle cells in the affected region will stop contracting almost immediately, leading to a reduced pumping function of the heart and a changed deformation pattern of the muscle. Characteristic electrical changes include reduced tissue conductivity and a disturbed balance between various ions, which affects the electrical potentials in the tissue. Arrhythmic activity may be a direct effect of the changes in the electrical properties, but it may also be caused by altered mechanical activity, through a process known as mechano-electric feedback, see e.g. Kohl and Ravens (2003) and Ravens (2003). Arrhythmia and fibrillation following a heart attack may therefore be caused by either electrical or mechanical changes in the tissue, or a combination of the two.

A striking example of the coupling between electrophysiology and mechanics is a phenomenon known as *commotio cordis*. As described in e.g. Nesbitt et al (2001), this term describes severe disturbance of the heart rhythm resulting from a relatively minor impact to the chest. Although rare, deaths caused by this phenomenon have occurred for instance in athletic activities such as baseball and soccer. A low-strength impact to the chest, causing no tissue damage, may result in electrical disturbances in the heart through mechano-electric feedback. If this occurs during a vulnerable period of the heart cycle, the result may be arrhythmic activity that rapidly evolve into fibrillation.

The acute treatment for ventricular fibrillation is the delivery of a large electric shock to the heart, a process known as defibrillation. If the shock is delivered within a few minutes after the onset of fibrillation, defibrillation has a remarkably high success rate, see e.g. Mckenzie (2004).

However, although it has been extensively studied over the last decades, the underlying mechanisms are not fully understood. Numerical simulations are seen as a promising tool to uncover some of the mechanisms underlying both cardiac arrhythmias and defibrillation. Although still in an early stage, mathematical models and simulations have already given researchers important new insight into these phenomena, see e.g. Keener (2004), Xie et al (2001) and Hillebrenner et al (2003).

Realistic simulations of heart activity are challenging, even if only considering a single cycle of normal heart activity. The electrical activity is characterized by rapid dynamics and steep spatial gradients, requiring high resolution in space and time to obtain satisfactory numerical solutions, see Lines et al (2003). The requirements are less severe for the equations describing the mechanical activity, but these models introduce other difficulties, in the form of severe non-linearities and complicated constitutive relations, see Holzapfel (2001) and Hunter et al (1998).

The challenges related to solving the electrophysiology equations become more serious when applying the models to study arrhythmia and defibrillation. To gain insight into the mechanisms of arrhythmias, it will often be necessary to run the simulations for a fairly long time interval, typically from a few seconds to several minutes. This substantially increases the computational load compared to simulating a single heart cycle, which only lasts about one second. Simulating the defibrillation shock leads to challenges of a different kind. The shock is normally applied for a very short time, typically from one to ten milliseconds, but during this time interval the electrical potentials reach values far beyond the normal physiological range. This is known to cause considerable numerical problems when solving the model equations. Time step restrictions in the order of microseconds have been reported, by Skoubine et al (2000) and Trayanova and Eason (2002). This leads to very time consuming simulations even if these restrictions apply only during the application of the shock.

The purpose of the present paper is to present an efficient algorithm for simulating arrhythmia and defibrillation. We mostly restrict the discussion to pure electrophysiology simulations, only briefly discussing models for mechano-electric coupling. The model considered is the bidomain model coupled to the Beeler-Reuter model for cellular kinetics. Although being relatively simple, the Beeler-Reuter model is suitable for many applications, and it can easily be coupled to contraction models in order to simulate the complete electro-mechanical process. The model is a non-linear system of PDEs and ODEs, for which we apply an operator splitting technique to separate the system into a system of linear PDEs and systems of non-linear ODEs. The PDE system is then discretized fully implicit in time with a backward Euler method, combined with a finite element space discretization. This leads to a block structured linear system, which is solved with a multigrid preconditioned conjugate gradient method. For solving the ODE systems resulting from the operator splitting process, we apply a singly diagonally implicit Runge-Kutta (SDIRK) method.

MODEL DESCRIPTION

The electrical activity in the heart is described by the bidomain model, derived by Tung (1978). This is a system of two PDEs coupled to systems of ODEs describing electro-chemical reactions in the cardiac cells. The models for cellular activity can be extended to include models for the active force generation in the muscle cells, which in turn may be coupled to a non-linear elasticity equation describing the movement of the heart muscle. The complete model can be

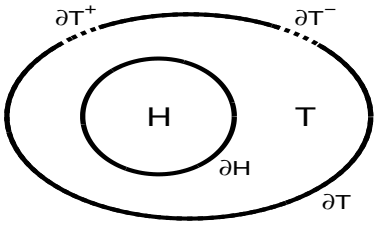

Fig. 1: A sketch of the heart embedded in a torso. Stapled lines indicate the location in which essential boundary conditions are set.

written as follows;

$$\frac{\partial s}{\partial t} = f(v, s, E) \qquad x \in H(t) \tag{1}$$

$$\frac{\partial v}{\partial t} + I_{\text{ion}}(v, s) = \nabla \cdot (M_i \nabla v) + \nabla \cdot (M_i \nabla u_e), \quad x \in H(t) \tag{2}$$

$$\nabla \cdot ((M_i + M_e)\nabla u_e) = -\nabla \cdot (M_i \nabla v), \qquad x \in H(t), \tag{3}$$

$$\nabla \cdot (M_T \nabla u_T) = 0, \qquad x \in T(t), \tag{4}$$

$$\nabla \cdot (FS) = 0 \qquad x \in H(0) \tag{5}$$

$$S = S^a(s) + S^p(E) \qquad x \in H(0) \tag{6}$$

$$S^p(E) = \frac{\partial W}{\partial E}, \qquad x \in H(0) \tag{7}$$

Eqs. (1)-(4) describe the electrical activity in the heart and the surrounding torso. The main variables are the transmembrane potential v, the extracellular potential u_e, and the vector s describing the state of the heart cells. Depending on the complexity of the cell model applied, s may contain from one to more than fifty elements. When the Beeler-Reuter model is used, s is a vector of seven variables, describing membrane gates and ionic concentrations. Furthermore u_T is the electrical potential in the torso surrounding the heart, which is described by a passive volume conductor model. The tensors M_i and M_e describe the intracellular and extracellular conductivities in the heart tissue, while M_T is the conductivity in the tissue surrounding the heart. For notational convenience the conductivities have been scaled, so that for $d = i, e, T$ we have

$$M_d = \frac{1}{C_m \chi} M_d^*,$$

where M_d^* is the physical conductivity, C_m is the capacitance of the cell membrane, and χ is the ratio of cell membrane area to tissue volume. A more detailed description of the bidomain model is given in Keener and Sneyd (1998) and in Lines et al (2003).

The heart moves, and (1)-(4) must therefore be formulated in time dependent domains $H(t)$ and $T(t)$. A sketch of the domains is given in Figure 1. We have only formulated the mechanics equations for the heart tissue, and it is therefore natural to assume that the boundary ∂H on the figure moves, while the outer boundary ∂T is fixed during the simulation. The electrophysiology equations are formulated relative to the deformed (current) configuration of the domain, and the computational grid must therefore be updated continuously to incorporate the movement of the muscle. Other formulations exist which enable computations on a fixed grid.

The mechanics of the heart muscle are described by (5)-(7). Eq. (5) describes the equilibrium of a material undergoing large deformations, where S is the second Piola-Kirchoff stress and F is the deformation gradient tensor, see e.g. Holzapfel (2001) for details. The active contraction of the muscle cells is included by splitting the stress tensor into an active and a passive part, as given by (6). The active part, being triggered by the electrical activation of the

tissue, is a function of the state vector s. Well known models for this part include for instance the HMT model, described in Hunter et al (1998). The passive stress is normally determined by treating the heart tissue as a hyper-elastic material, where the components of the stress tensor are computed as partial derivatives of a given strain energy function W with respect to the Green-Lagrange strain E, see (7). The strain energy function defines a constitutive law for the material, see e.g. Hunter et al (1998) and Usyk et al (2002) for examples. Inserting the constitutive relation in (5), along with the expression for the Green-Lagrange strain, leads to a non-linear equation system which may be solved for the tissue displacements, see e.g. Holzapfel (2001) for details.

The model described above is suitable for describing the two-way coupling between electrical activity and mechanics. As described above the active part of the stress is a function of s, which provides one direction of the coupling. The mechano-electric feedback, which is typically mediated by so-called stretch activated channels, is included through the occurrence of the strain tensor E in the right hand side of (1).

The way they are formulated above, the mechanics equations are referred to the original (reference) configuration of the heart muscle. These equations may there fore be solved for a fixed domain, and the solution may be used to update the time dependent domains $H(t)$ and $T(t)$ for the electrophysiology computations. In the numerical experiments presented below we will only consider the electrophysiology equations. The mechanics and movement of the heart muscle will not be considered, and all computations are therefore performed on static domains.

Boundary conditions

The model described above must be completed with boundary conditions. For the electrophysiology equations we need boundary conditions on the heart-torso interface and on the outer surface of the body, while the mechanics equations require boundary conditions on the heart surface.

On the boundary of H, we apply the original boundary conditions proposed by Tung (1978). The intracellular space is assumed to be completely insulated from the surrounding tissue, implying that the normal component of the intracellular current is zero on ∂H. Using that $u_i = u_e + v$, see e.g. Keener and Sneyd (1998), this yields

$$(M_i \nabla v + M_i \nabla u_e) \cdot n_H = 0. \tag{8}$$

Furthermore, the extracellular tissue is assumed to be directly connected to the tissue surrounding the heart. This implies that both the electrical potential and the current in these domains must be continuous across ∂H. We have

$$u_e = u_T, \tag{9}$$

and

$$(M_e \nabla u_e) \cdot n_H = -(M_T \nabla u_T) \cdot n_T, \tag{10}$$

on ∂H. Note that the unit normal n_T occurring on the right hand side is the outward unit normal of T on ∂H, which points into the heart domain H.

For normal simulations of cardiac electrical activity it is common to assume that the body is completely insulated from its surroundings, which yields the no-flux condition

$$(M_T \nabla u_T) \cdot n_T = 0. \tag{11}$$

However, in order to simulate defibrillation shock this condition has to be modified, since the defibrillation electrodes will typically be applied to ∂T. These are incorporated by dividing the outer boundary in three parts, see Figure 1, and applying essential boundary conditions on the parts ∂T^+ and ∂T^-. We have

$$u_T = \begin{cases} +u_{app} & \text{in } \partial T^+ \\ -u_{app} & \text{in } \partial T^- \end{cases} \tag{12}$$

so that ∂T^+ becomes the anode, and ∂T^- the cathode, see Figure 1 for an illustration. We will investigate the outcome of several shock strengths in our simulations.

The boundary conditions for the mechanics equations are intended to mimic the way the heart is attached inside the torso, as well as the effect of the blood flow in the heart cavities. The characteristics of the blood flow change during the heart cycle. As described in Usyk et al (2002) this can be incorporated through time dependent boundary conditions, which are adjusted to emulate the various phases of the heart cycle. The result is a fairly complicated system of boundary conditions for the elasticity equations. The main focus of the present work is on the electrophysiology equations, and we refer to Usyk et al (2002) for the boundary conditions for the mechanics problem.

The Beeler-Reuter cell model

The kinetics of the cell membrane are described here by a modified Beeler-Reuter model, see Beeler and Reuter (1977). We will in the following only consider electrophysiology simulations, not including mechano-electric effects such as stretch activated channels in the model. The model is a system of ODEs which includes update of the intracellular calcium concentration and six gating variables in addition to the transmembrane potential. We denote the gates by $y = k, m, h, l, f, d$, and these all obey ODEs on the form

$$\frac{dy}{dt} = \alpha_y(1 - y) - \beta_y y,$$

with $\alpha_y(v)$ and $\beta_y(v)$ being respectively the opening and closing rates of the membrane channel. For convenience, the calcium concentration is scaled like $c = 10^7[Ca]_i$, such that c satisfies

$$\frac{dc}{dt} = 0.07(1 - c) - I_{si}(v, c, f, d),$$

where I_{si} is an outward current, mainly consisting of calcium ions, and reads

$$I_{si}(v, c, f, d) = g_{si} f d(v + 82.3 + 13.0287 \ln(10^{-7} c)).$$

Flow of sodium (Na) ions is described by a second outward current, and is given by

$$I_{Na}(v, m, h, l) = (g_{Na} m^3 h l + g_{NaC})(v - v_{Na}),$$

where g_{Na} is the conductivity of the cell membrane related to sodium, and v_{Na} is the equilibrium potential of that current. The potassium flow is modeled by an inward two component current; one time dependent and one independent of time, respectively given by

$$I_k(v, k) = 0.8k \frac{e^{0.04(v+77)} - 1}{e^{0.04(v+35)}},$$

and

$$I_K(v) = 1.4 \frac{e^{0.04(v+77)} - 1}{e^{0.08(v+53)} + e^{0.04(v+53)}}.$$

In order to handle strong electric fields, the cell model needs to be modified. We do this in a fashion similar to that of Skouibine et al (2000), and introduce G as the electroporation function obeying

$$\frac{dG}{dt} = \alpha e^{\beta(v - v_r)^2}(1 - e^{-\gamma(v - v_r)^2}),$$

where α, β and γ are constants, and the potential at rest is set to $v_r = -84.35$. Then the total ionic current reads

$$I_{\text{ion}}(v, s) = I_{si}(v, f, d, c) + I_{Na}(v, m, h, l) + I_K(v) + I_k(v, k) + Gv.$$

The electroporation function models the effect of the shock on the pores of the cell membrane, see e.g. Krassowska (1995) for details. The adjustments are well described in Skouibine et al (2000). In that paper, the update of the intracellular calcium concentration c, is turned off for $v > 200\text{mV}$ to prevent c from becoming negative. This is a limitation due to numerical instability, since the term describing flow of Ca^{2+}-ions includes a logarithmic function. However, our simulation results show that the Ca-concentration becomes negative for $v \geq 180\text{mV}$ when $\Delta t = 0.1\text{ms}$, and thus the numerical method diverges. However, we have observed convergence for $\Delta t \leq 0.07\text{ms}$, even with the calcium change turned off for v above 200mV.

NUMERICAL METHOD

The complete model (1)-(7) is a highly complex system of ODEs and PDEs, and operator splitting techniques stand out as attractive methods for splitting this system into more manageable parts. We here present such a technique for solving the electrophysiology equations (1)-(4), with boundary conditions (8)-(12). We only give a brief outline of the procedure, whereas for a detailed description, we refer to Sundnes et al (2005) and the references therein.

A Godunov splitting technique is used to split the non-linear system into linear PDEs and non-linear ODEs. Assuming that the solution is known at time t^n, the solution at the next time step is computed with the following steps;

Step 1. Solve the ODE system

$$\begin{aligned} \partial_t v &= -I_{ion}(v, s) \\ \partial_t s &= F(v, s) \end{aligned}$$

for $t^n < t \leq t^n + 1$, to obtain s^{n+1} and a temporary update v^* for v.

Step 2 Solve the linear PDE system

$$\begin{aligned} \tfrac{\partial v}{\partial t}\nabla \cdot (M_i \nabla v) + \nabla \cdot (M_i \nabla u_e) &= \nabla \cdot (M_i \nabla v) + \nabla \cdot (M_i \nabla u_e), & x \in H, \\ \nabla \cdot (M_i \nabla v) + \nabla \cdot ((M_i + M_e)\nabla u_e) &= 0, & x \in H, \\ \nabla \cdot (M_T \nabla u_T) &= 0, & x \in T, \end{aligned}$$

for $t^n < t \leq t^{n+1}$, using the value v^* from Step 1 as initial condition for v. The result is a first order approximation to v, u_e and u_T at time t^{n+1}.

Although the systems resulting from the operator splitting technique are considerably simpler than the original system, the equations in Step 1 and Step 2 must still be solved with numerical techniques. For the ODE systems in Step 1 we apply a singly diagonally implicit Runge-Kutta (SDIRK) method, whereas for the PDE discretization we use a backward Euler time discretization combined with a Galerkin finite element method. This leads to a linear system of the form

$$\mathcal{A} \begin{bmatrix} v_h \\ u_h \end{bmatrix} = \begin{bmatrix} A & B \\ B^T & C \end{bmatrix} \begin{bmatrix} v_h \\ u_h \end{bmatrix} = \begin{bmatrix} \alpha \\ \beta \end{bmatrix}, \tag{13}$$

to be solved for each time steps. Here v_h is a vector containing the unknown nodal values of v, while the vector u contains the nodal values of both u_e and u_T. The blocks are defined by

$$\begin{aligned} A_{jk} &= \textstyle\int_H \psi_j \psi_k dx + \Delta t \int_H M_i \nabla \psi_j \cdot \nabla \psi_k dx, \\ B_{jk} &= \Delta t \textstyle\int_H M_i \nabla \psi_j \cdot \nabla \eta_k dx, \\ C_{jk} &= \Delta t \textstyle\int_H (M_i + M_e) \nabla \eta_j \cdot \nabla \eta_k dx + \int_T M_T \nabla \eta_j \cdot \nabla \eta_k dx, \\ \alpha_j &= \textstyle\int_H \psi_j v^n dx - \Delta t \int_H M_i \nabla \psi_j \cdot \nabla v^n dx, \\ \beta_j &= 0, \end{aligned}$$

for suitable test functions ψ_j and η_j defined over the domains H and $H \cup T$, respectively.

The entries in β will only be zero if no essential boundary conditions are applied. When incorporating the electric shock in the form of essential boundary conditions, the linear system is

adjusted so that β gets non-zero entries. A multigrid preconditioned conjugate gradient method is applied in order to solve the system (13), see Sundnes et al (2005) for details of this procedure.

SIMULATIONS AND RESULTS

The steep gradients due to the electric shock normally require extremely small time steps. Trayanova and Eason (2002) have used a temporal step size of $5\mu s$. We here present experiments investigating the largest time step allowed by the operator splitting method presented above. Table 1 shows the maximum time step for which the algorithm converges during the shock. We observe that the convergence improves as the shock strength decreases; going from a shock strength of 16.67 V/cm to 10.0 V/cm doubles the value of Δt that gives convergence.

Shock strength (V/cm)	Δt_{max}(ms)
16.67	0.24
16.0	0.26
15.0	0.3
12.0	0.36
10.0	0.48

Table 1: Table of maximum value of time step for different shock strength of duration $10ms$. The solver converges within 7 iterations on average.

Table 2 shows the number of iterations for different number of nodes on the square geometry shown in Figure 2. The heart occupies the region $[0, 1] \times [0, 1]$, while the surrounding region is the passively conducting torso. A reentrant spiral wave is introduced in the heart, and the shock is then applied as essential boundary conditions on the boundaries $y = -2$ and $y = 4$. The convergence criterion used is based on the absolute residual of the iterative solver. We observe, from Table 2, nearly optimal convergence, both with and without the essential boundary conditions set. Notice from Figure 2 that the steep gradients that occur during shock (right part) totally dominate the picture, as opposed to the situation under normal conditions (left part).

nodes	without shock	during shock
16 384	7	11
65 536	9	13
262 144	10	14

Table 2: Number of iterations for different number of grid levels.

Simulations have also been run on a more realistic 2D geometry, resembling a cross section of the heart and the torso. The cardiac tissue is initially stimulated, in order for a left-going wave to propagate for 30ms. Then we set a shock, on the surface of the torso, of strength 10.0V/cm and 10ms duration. Figure 3 shows the torso (left) as well as the heart (right) that are subjuct to strong electric fields. In Table 3 we run tests on this grid for several shock strengths, using four grid levels. We see that the number of iterations increases significantly during the application of the shock. This is partly due to the convergence criterion used, which is based on the absolute residual. Since the magnitude of the solution increases dramatically during the shock, this criterion becomes very strict. A convergence criterion relating the residual to the magnitude of the solution may be more appropriate in this case.

As a final test example we simulate a defibrillation shock applied to a heart suffering from reentrant arrhythmia. We use the simple square geometry, and induce a reentrant spiral wave using an S1-S2 stimulus protocol. The very right end of the cardiac tissue slice is first stimulated

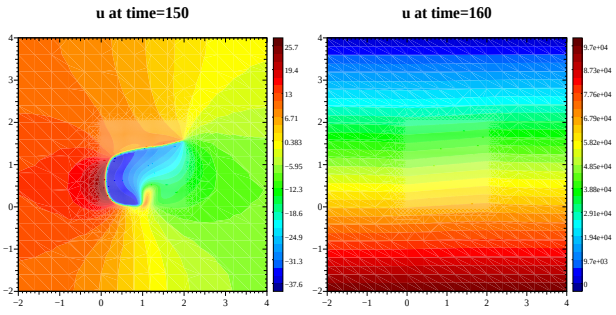

Fig. 2: Left panel: Plot of a square torso embedding a heart with a reentrant spiral wave. Right panel: Torso during defibrillation shock.

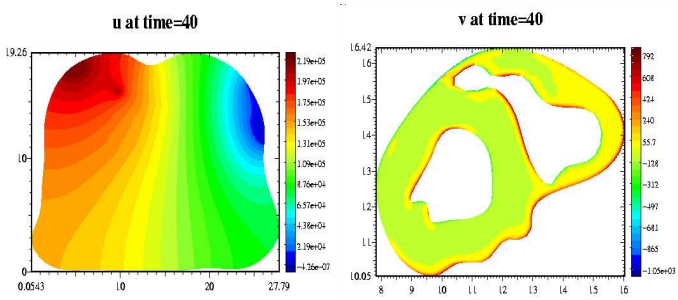

Fig. 3: A slice of body and heart undergoing electric shock.

Shock strength ($\frac{V}{cm}$)	before shock	onset of shock	during shock
9.1	11	49	32
13.7	11	50	32
16.4	11	51	32

Table 3: Number of iterations for several shock strengths before, at onset of and during shock.

for 1 ms to produce a left-going wave. Then, 130ms later, an S2 stimulus, also of 1 ms duration, is initiated in the right lower corner of the myocardial tissue. By now, the first wave is in its refractory period, causing the S2 wave to propagate unevenly in the vertical direction, whereas the horizontal propagation is blocked. The result is a sustained reentry wave that propagates in the tissue. See Figure 4 for spiral wave birth and evolvement.

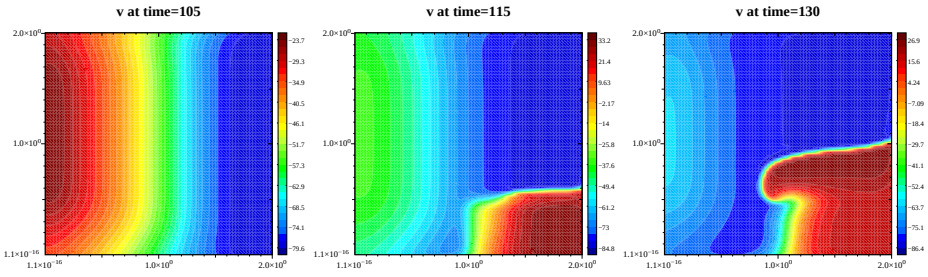

Fig. 4: Left: Wave $S1$ propagation 105ms after onset. Middle: Refractory state of S1-wave results in one-sided block of S2 stimulus. Right: Spiral wave propagation throughout the tissue.

At 150ms after the onset of s1, we set a shock of strength 16.67V/cm of 10ms duration, see

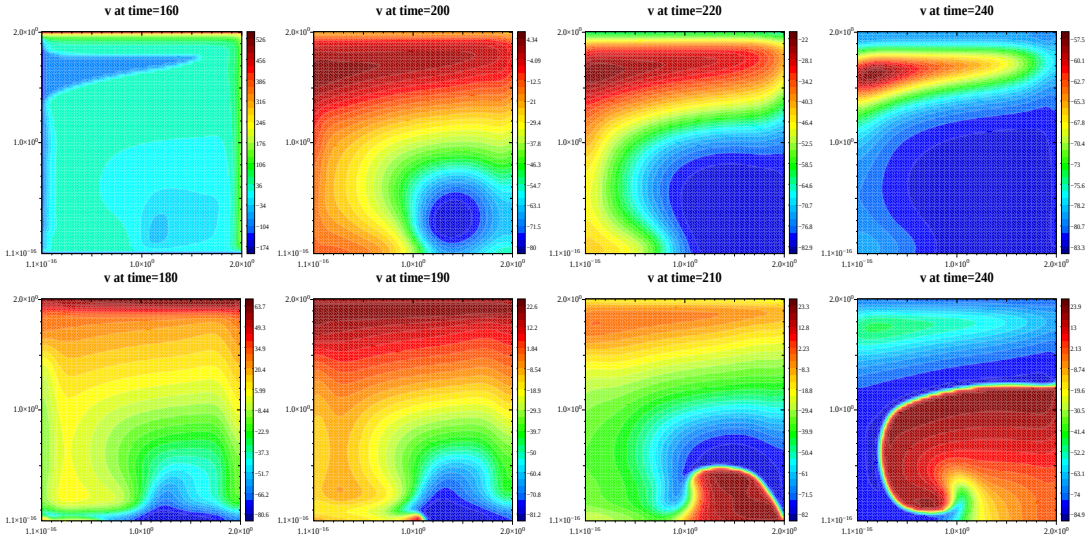

Fig. 5: Top row: Plot of transmembrane potential during and after onset of shock of strength 16.67 V/cm and 10ms duration. Bottom row: Evolvement of v during and after onset of shock of strength 5 V, also 10ms duration.

top row of Figure 5. This corresponds to values of respectively $u_T = 200$ V and $u_T = 0$ V for the cathode and the anode. A large part of the tissue is depolarized, making it impossible for new waves to propagate for several milliseconds. At time $t = 240$ms, a large part of the tissue is repolarized, and the heart will soon be ready for normal stimulation. This simulation hence demonstrates a successful defibrillation shock, as all reentrant activity was removed, and no new reentrant waves were generated by the shock. The bottom row of Figure 5 shows a similar experiment with a weaker defibrillation shock, of strength 5 V/cm, also lasting for 10ms. It is seen at the bottom of the tissue a new rotor that will evolve and stabilize, and thus the defibrillation attempt failed.

CONCLUSION AND FURTHER WORK

In this paper we have presented a method for solving the bidomain equations with application to cardiac defibrillation. The solver has been adjusted to handle essential boundary conditions which serve as external electrodes set on the surface of the body. Initial experiments indicate that the numerical method used is fairly stable, allowing larger time steps than what is previously reported in the literature. The results of the simulations seem to be in accordance with results reported by other researchers in the field.

The experiments presented in this paper are fairly limited, in that we only consider 2D geometries. More experiments must be performed, preferably on realistic 3D geometries, to determine if the proposed numerical method is suitable for practical defibrillation simulations. Another important step is to combine the given algorithm with a solver for the mechanics equations, to be able to perform complete electro-mechanics simulations. This will enable us to investigate the role of different mechanisms in the the development of cardiac arrhythmias.

REFERENCES

Beeler, G. W. and Reuter, H. (1977). Reconstruction of the action potential of ventricular myocardial fibres. *J. of Phys.*, 268:177–210.

Chen, P. S., Wu, T. J., Ting, C. T., Karagueuzian, H. S., Garfinkel, A., Lin, S. E., and Weiss, J. N. (2003). A tale of two fibrillations. *Circulation*, 108:2298–2303.

Hillebrenner, M. G., Eason, J., and Trayanova, N. (2003). Mechanistic inquiry into decrease in probability of defibrillation success with increase in complexity of preshock reentrant activity. *Am J Physiol Heart Circ. Physiol.*, 286:H909–917.

Holzapfel, G. (2001). *Nonlinear solid mechanics: A continuum approach for engineering*. John Wiley & Sons.

Hunter, P., McCulloch, A., and ter Keurs, H. (1998). Modelling the mechanical properties of cardiac muscle. *Biophy & Molec. Biol.*, 69:289–331.

Keener, J. and Sneyd, J. (1980). Mathematical physiology, volume 8. Springer.

Keener, J. P. (2004). The topology of defibrillation. *J Theor Biol*, 21:459–473.

Kohl, P. and Ravens, U. (2003). Mechano-electric feedback: past, present and prospect. *Progress in biophysics and molecular biology*, 82:3–9.

Krassowska, W. (1995). Effects of electroporation on transmembrane potential induced by defibrillation shocks. *PACE*, 18:1644–1660.

Lines, G. T., Buist, M. L., Grøttum, P., Pullan, A. J., Sundnes, J., and Tveito, A. (2003). Mathematical models and numerical methods for the forward problem in cardiac electrophysiology. *Computations and Visualization in Science*, 5:215–239.

Mackenzie, D. (2004). Making sense of a heart gone wild. *Science*, 303:786–787.

Nesbitt, A., Cooper, P. J., and Kohl, P. (2001). Rediscovering commotio cordis. *The Lancet*, 357:1195–1197.

Ravens, U. (2003). Mechano-electric feedback and arrhythmias. *Progress in biophysics and molecular biology*, 82:255–266.

Skouibine, K., Trayanova, N., and Moore, P. (2000). A numerically efficient model for simulation of defibrillation in an active bidomain sheet of myocardium. *Mathematical Biosciences*, 166:85–100.

Sundnes, J., Lines, G. T., and Tveito, A. (2005). An operator splitting method for solving the bidomain equations coupled to a volume conductor model for the torso. *Mathematical Biosciences*.

Trayanova, N. and Eason, J. (2002). Shock-induced arrhythmogenesis in the myocardium. *Chaos*, 12:Number 3.

Tung, L. (1978). A bi-domain model for describing ischemic myocardial d-c potentials. *Ph. D. thesis. MIT, Cambridge, MA:*.

Usyk, T., LeGrice, I., and McCulloch, A. (2002). Computational model of three-dimensional cardiac electromechanics. *Computations and Visualization in Science*, 4:249–257.

Xie, F., Qu, Z., Garfinkel, A., and Weiss, J. N. (2001). Electrophysiological heterogeneity and stability of reentry in simulated cardiac tissue. *Am J Physiol Heart Circ Physiol*, 280:H535–H545.